ResearchGate

See discussions, stats, and author profiles for this publication at: https://www.researchgate.net/publication/280932544

Role of Li2O2@Li2CO3 Interfaces on Charge Transport in Nonaqueous Li–Air Batteries

ARTICLE *in* THE JOURNAL OF PHYSICAL CHEMISTRY C · JULY 2015

Impact Factor: 4.77 · DOI: 10.1021/acs.jpcc.5b04432

CITATION
1

READS
23

1 AUTHOR:

Yedilfana Setarge Mekonnen
Technical University of Denmark
4 PUBLICATIONS **11** CITATIONS

SEE PROFILE

Available from: Yedilfana Setarge Mekonnen
Retrieved on: 16 January 2016

THE JOURNAL OF PHYSICAL CHEMISTRY C

Article

pubs.acs.org/JPCC

Role of Li_2O_2@Li_2CO_3 Interfaces on Charge Transport in Nonaqueous Li−Air Batteries

Yedilfana S. Mekonnen,[†] Juan M. Garcia-Lastra,[†] Jens S. Hummelshøj,[§] Chengjun Jin,[‡] and Tejs Vegge*[,†]

[†]Department of Energy Conversion and Storage, Technical University of Denmark, Fysikvej, Building 309, 2800 Kgs Lyngby, Denmark

[‡]Center for Atomic-Scale Materials Design and Department of Physics, Technical University of Denmark, Fysikvej, Building 307, 2800 Kgs Lyngby, Denmark

[§]SUNCAT Center for Interface Science and Catalysis, SLAC National Accelerator Laboratory, Menlo Park, California 94025, United States

ABSTRACT: The formation and oxidation of the main discharge product in nonaqueous secondary Li−O_2 batteries, that is, Li_2O_2, has been studied intensively, but less attention has been given to the formation of cathode−electrolyte interfaces, which can significantly influence the performance of the Li−O_2 battery. Here we apply density functional theory with the Hubbard U correction (DFT+U) and nonequilibrium Green's function (NEGF) methods to investigate the role of Li_2O_2@Li_2CO_3 interface layers on the ionic and electronic transport properties at the oxygen electrode. We show that, for example, lithium vacancies accumulate at the peroxide part of the interface during charge, reducing the coherent electron transport by two to three orders of magnitude compared with pristine Li_2O_2. During discharge, Li_2O_2@Li_2CO_3 interfaces may, however, provide an alternative in-plane channel for fast electron polaron hopping that could improve the electronic conductivity and ultimately increase the practical capacity in nonaqueous Li−O_2 batteries.

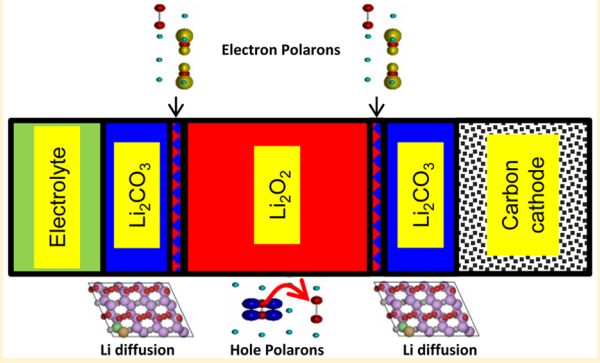

1. INTRODUCTION

Today, most electric vehicles and hybrid electric vehicles rely on Li-ion batteries. The main drawbacks of Li-ion batteries are their high price, slow charging, and low energy/power density compared with that of gasoline.[1] The latest specific energy of Li-ion batteries is ∼300 mAh/g,[2] which is an order of magnitude lower than that of the Li−air battery, ∼3842 mAh/g.[3] Recently, metal−air batteries have gained significant attention as a future alternative to Li-ion batteries in the transportation sector. In particular, the Li−O_2 couple appears to be a promising choice due to its superior energy storing capacity.

Li−air batteries, however, suffer from several drawbacks that must be resolved before they can enter the market. Various complex chemical and electrochemical side-reactions occur at the interfaces in practical nonaqueous Li−air batteries, which limits the rechargeability and cyclability.[4] Several kinds of parasitic compounds and interfaces are likely formed between/within the reaction products and cell components in the nonaqueous Li−air batteries. The types of interfaces depend on the type of electrodes and electrolytes used in the cell and the reaction conditions. Li_2CO_3 is readily formed at the cathode together with Li_2O_2 when carbonate-based electrolytes, for example, ethylene carbonates (ECs), are used,[5,6] but if noncarbonate-based electrolytes such as dimethoxyethane (DME) are used, Li_2O_2 is the main discharge product. In the latter case, layers of Li_2CO_3 can also form due to side reactions with the carbon cathode, DME, or CO_2 impurities from the air.[7,8] The discharge capacity in Li−O_2 batteries is primarily limited by the poor electronic conduction in Li_2O_2[9] and because electronic conductivity in Li_2CO_3 is even smaller than that of Li_2O_2, it is critical to determine the effect of such layers. Experiments performed in carbon- or ether-based electrolytes reported that the evolution of CO_2 gas when the battery recharges at slightly above 3 and 4 V mainly comes from the electrolyte decomposition and carbonate deposit at the cathode surface, respectively.[4,6,8,10] It has also been reported in Li-ion battery studies that Li_2CO_3 is one of the most chemically[11] and mechanically[12] stable species formed at both cathode and anode electrodes. Thus, it is inevitably the formation of Li_2O_2@Li_2CO_3 interfaces in the cathode of nonaqueous Li−air batteries, for instance, at Li_2O_2@C(graphite) and Li_2O_2@electrolyte interfaces.[4] To summarize, Li_2O_2@Li_2CO_3 interfaces could be formed in different scenarios, namely, (a) liquid electrolyte |Li_2CO_3|Li_2O_2| carbon cathode, which appears when a carbon-based electrolyte is used or due to the presence of atmospheric CO_2; (b) liquid electrolyte |Li_2O_2|Li_2CO_3| carbon cathode, which has been shown to be formed due to the

Received: May 8, 2015
Revised: June 24, 2015
Published: July 20, 2015

ACS Publications © 2015 American Chemical Society

DOI: 10.1021/acs.jpcc.5b04432
J. Phys. Chem. C 2015, 119, 18066−18073

reactions between the Li ions and C cathode in the presence of oxygen; and (c) liquid electrolyte $|Li_2CO_3|Li_2O_2|Li_2CO_3|$ carbon cathode, which is the combination of the above scenarios a and b. We should stress that in the present work we only model the Li_2O_2@Li_2CO_3 interface, disregarding where the interface appears. Thus, our model is valid in the three scenarios previously mentioned.

Here we investigate the implications of Li_2O_2@Li_2CO_3 interfaces for charge transport, that is, mainly the lithium diffusion and electronic transport properties in nonaqueous Li–O_2 batteries.[13] Regarding, the electronic transport we study both polaronic and tunneling conduction regimes. We also show that the Li vacancies have a thermodynamic driving force for accumulation at the Li_2O_2 part of the Li_2O_2@Li_2CO_3 interface compared with pristine Li_2O_2. Consequently, we have studied in detail the impact of these Li vacancies on the coherent transport properties at the interface.

The paper is structured in four major sections. The description of the crystal structures, computational methods, and electronic properties of the materials is covered in Section 2. In Section 3, the main results are discussed in three subsections. The first subsection (3.1) covers the ionic transport calculations in the materials of interest in nonaqueous Li–air batteries, that is, Li_2O_2, Li_2CO_3, and Li_2O_2@Li_2CO_3 interface. The coherent electron transport properties with and without lithium vacancies in Li_2O_2 and Li_2O_2@Li_2CO_3 interface are discussed in subsection 3.2, while the polaronic conduction in the Li_2O_2@Li_2CO_3 interface is detailed in subsection 3.3. Finally, we present our main conclusions in Section 4.

2. CRYSTAL STRUCTURES AND COMPUTATIONAL METHODS

Li_2O_2 crystallizes in a hexagonal crystal structure with lattice parameters $a = b = 3.187$ Å, $c = 7.726$ Å (space group $P6_3/mmc$, see Figure 1a), and it can effectively be viewed as individual peroxide O_2^{2-} ions embedded in sea of Li^+ ions.[14−16]

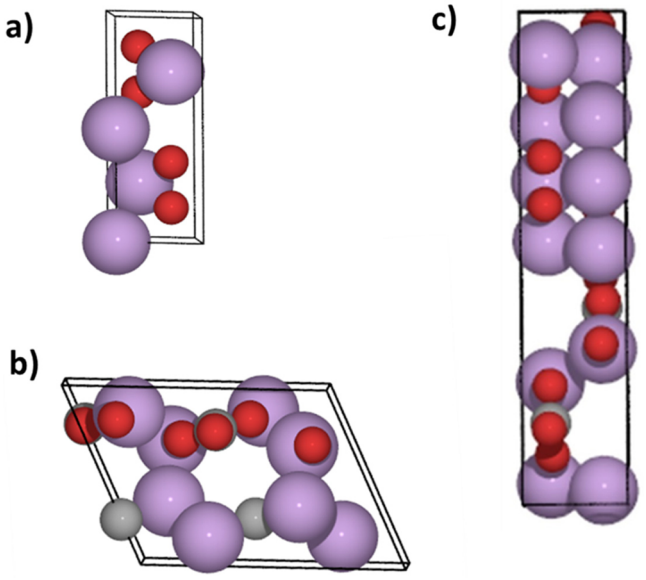

Figure 1. (a) Hexagonal Li_2O_2 structure with lattice parameters $a = b = 3.187$ Å and $c = 7.726$ Å (space group $P6_3/mmc$). (b) Monoclinic Li_2CO_3 structure with space group 15 ($C2/c$) with lattice parameters $a = 8.359$ Å, $b = 4.973$ Å, $c = 6.197$ Å, and $\beta = 114.83°$. (c) Interface, Li_2O_2@Li_2CO_3, with 4.8% strains on Li_2O_2.

Moreover, in previous DFT calculations it has been reported that the reconstructed (0001), $(1\bar{1}00)$, and $(1\bar{1}20)$ surfaces are the most stable and predominant exposed facets at operating potentials, being ~80% dominated by (0001) surface.[17,18]

The monoclinic Li_2CO_3 crystal structure with space group $C2/c$ (see Figure 1b) consists of four formula units per unit cell with lattice parameters $a = 8.359$ Å, $b = 4.973$ Å, $c = 6.197$ Å, and $\beta = 114.83°$.[19] The planar CO_3^{-2} groups with C–O bond lengths of 1.284, 1.305, and 1.305 Å are surrounded by the sea of Li^+ ions. The Li^+ and CO_3^{-2} groups are oriented alternatively on the XY plane. Each Li^+ ion is coordinated with four oxygens to form a tetrahedral structure.

The Li_2O_2@Li_2CO_3 interface explored in this study is assembled from Li_2CO_3 (adopting a two formula unit cell version of a Li_2CO_3 crystal structure) and Li_2O_2 (adopting a four formula unit cell). The interface is built from a (0001) facet of Li_2O_2 and a (011) facet of Li_2CO_3 with lattice parameters $a = 5.135$ Å, $b = 6.918$ Å, and $c = 16.165$ Å (see Figure 1c). In both components, oxygen-terminated surfaces are used. In the Li_2CO_3 part of the interface, the planes of the carbonate groups are aligned parallel to the peroxides along the z axis. The facets are chosen based on their stability and presence in the discharge products: The (0001) facet is one of the most stable and predominant facets (80%) on Li_2O_2 around the equilibrium potential during discharge and charge in nonaqueous Li–air batteries, with an abundant portion of the oxygen-rich (0001) surface at potentials suitable for charging.[17,18,20] Moreover, the Li_2CO_3(011) surface is one of the low-energy facets,[21] which has an excellent lattice matching with Li_2O_2 (0001). As it can be seen in Figure 1c, the two facets match well and form a stable interface with <5% lattice mismatch (the strain is on Li_2O_2). This setup of the interface contains a relatively small number of atoms (the unit cell contains 28 atoms), which makes the calculations tractable and at the same time provides a reliable description of the interface.

Regarding the polarons and Li vacancy migration studies, all of the calculations are performed within density functional theory (DFT),[22,23] as implemented in the GPAW package[24,25] combined with the Atomic Simulation Environment (ASE).[26] The package uses a real-space grid algorithm based on the projector-augmented wave function method[27] with the frozen core approximation. The revised Perdew–Burke–Ernzehof (RPBE) exchange correlation functional is used in all calculations.[28] For bulk Li_2O_2, we use a 3 × 3 × 1 supercell (72 atoms) with a 3 × 3 × 3 k-point sampling. For bulk Li_2CO_3, we employ a 2 × 2 × 2 supercell (192 atoms) with a 1 × 2 × 2 k-point sampling. The calculations of the ionic transport in the Li_2O_2@Li_2CO_3 interface are carried out using the setup previously described (Figure 1c) with 2 × 2 × 1 k-point sampling (112 atoms in the supercell) to minimize the electrostatic interactions between replicas. A similar supercell size is implemented for the polaronic transport calculations study in the Li_2O_2@Li_2CO_3 interface.

It has been previously reported that it is necessary to introduce Hubbard corrections to the DFT Hamiltonian to describe properly the localization of polarons using general gradient approximation (GGA) functionals. Following previous works in our group, we use a $U = 6$ eV Hubbard correction applied on the 2p orbitals of carbon and oxygen atoms

The energy barrier, E_b, in both the lithium diffusion and polaronic (hole and electron) hopping is calculated using the climbing image nudged elastic band method (CI-NEB).[29−31] All ground-state energies are determined when Hellmann–

DOI: 10.1021/acs.jpcc.5b04432
J. Phys. Chem. C 2015, 119, 18066−18073

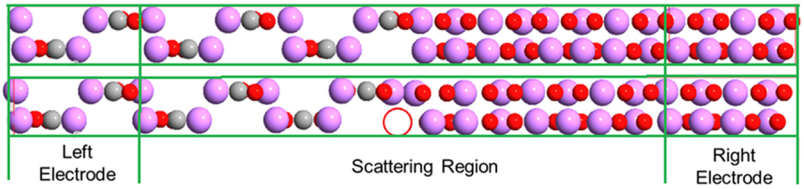

Figure 2. Structural setup for the device region for the pristine interface Li_2O_2@Li_2CO_3 (upper) and with a Li vacancy at the peroxide part of the interface, Li_2O_2 vac@Li_2CO_3 (lower).

Feynman forces are <0.03 eV/Å. All of the atoms in the supercell are free to relax during the optimization. From the computed E_b, it is possible to obtain the rate (r) and the diffusion coefficient (D) using the relations $r = \nu e^{-E_b/k_BT}$ and $D = a^2 r$, respectively, where ν is the hopping rate (in this work we use $\nu = 10^{13}$ s^{-1}) and a is the jump length.

The coherent electronic transport calculations in the tunneling regime are carried out using the Nonequilibrium Green's function (NEGF) formalism. The calculations are performed using a localized linear combination of atomic orbitals (LCAO) basis set (double-ζ plus polarization quality basis for all atomic species), as implemented in the Atomistix ToolKit (ATK)[32−34] package, where a central device region (or scattering region) is connected to two semi-infinite leads, which are kept at fixed electronic chemical potentials, μ_L and μ_R, respectively, to simulate an applied bias voltage across the device region given by $V = (\mu_L - \mu_R)/e$. The scattering region describing the Li_2O_2@Li_2CO_3 interface contains four formula units of Li_2CO_3 and eight formula units of Li_2O_2. The electrode regions consist of two formula units of bulk Li_2CO_3 (left lead) and four formula units of Li_2O_2 (right lead). For the sake of consistency, RPBE exchange correlation functional is employed. A 4 × 6 × 100 k-point sampling is used during the NEGF self-consistent loop. In the finite bias calculations, a positive bias is defined as sending electrons from the left lead to the right lead (see Figure 2).

3. RESULTS AND DISCUSSION

Here the main results and discussions are presented in three subsections as shown later. The first subsection (3.1) covers the ionic transport calculations in the bulk Li_2O_2, Li_2CO_3, and Li_2O_2@Li_2CO_3 interface. The coherent electron transport properties with and without lithium vacancies in Li_2O_2 and Li_2O_2@Li_2CO_3 interface are discussed in subsection 3.2, while the polaronic conduction in the Li_2O_2@Li_2CO_3 interface is detailed in subsection 3.3.

3.1. Ionic Transport in Li_2O_2, Li_2CO_3, and Li_2O_2@Li_2CO_3 Interface. In this subsection, the details of the lithium vacancy diffusion in bulk Li_2O_2, Li_2CO_3, and Li_2O_2@Li_2CO_3 interface across various pathways are discussed. Lithium vacancies, V^0_{Li}, are modeled by removing a single Li atom from a supercell and subsequently relaxing the system internally. Here we analyze the effect of neutral vacancies, but positive (V^{+1}_{Li}) and negatively charged vacancies (V^{-1}_{Li}) can also be present, depending on the potential.[35] For lithium diffusion studies, a single Li atom is removed from the corresponding supercells with a total vacancy concentration [V^0_{Li}] of 2.78, 1.6, and 2% in the peroxide, carbonate, and interface systems, respectively. We have checked that the formation energy of a second [V^0_{Li}] vacancy in all of the systems is practically the same as that of the first [V^0_{Li}] vacancy; that is, the formation energy of the vacancies is nearly independent of their concentration.

In Li_2O_2, there are four possible inequivalent hops in the intralayer direction (in the XY plane, see Figure 4), namely,

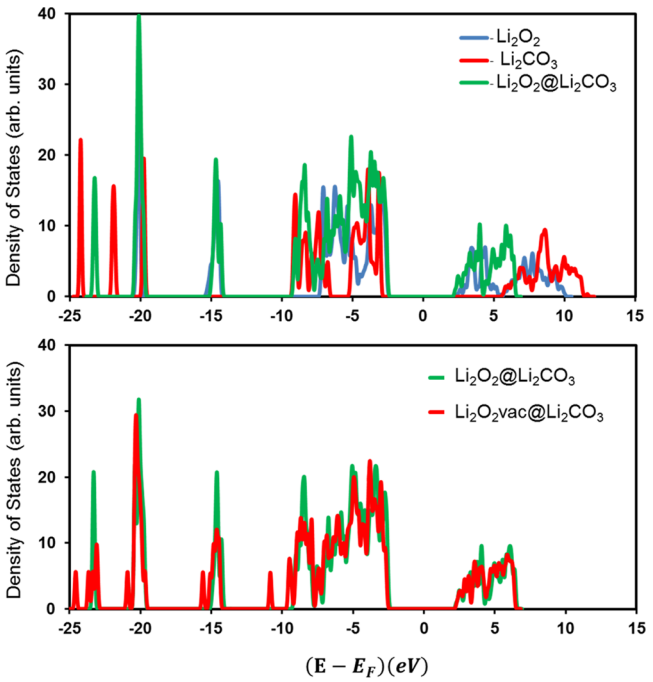

Figure 3. Total density of states (DOS) relative to the Fermi energy for (a) pristine Li_2O_2, Li_2CO_3, and Li_2O_2@Li_2CO_3 and (b) pristine Li_2O_2@Li_2CO_3 and with a defect (neutral Li vacancy, V^0_{Li}) at the peroxide part of the interface Li_2O_2 vac@Li_2CO_3 is obtained using RPBE + U (U = 6 eV).

BE(X) and AD(X) in the X direction and AF(Y) and BG(Y) in the Y direction, being in all of the cases the energy barriers close to 1 eV. Regarding the interlayer diffusion (in Z direction), there are two possible inequivalent hops, namely, AB(Z) and BC(Z). We find E_b = 0.44 eV and the E_b = 0.36 eV for AB(Z) hop and BC(Z) hop, respectively, giving an average E_b = 0.40 eV. Thus, it is clear that V^0_{Li} diffusion has a preferential channel in the Z direction. The microscopic diffusion channel follows A → B → C series along the Z direction with an average rate of $r = 2 \times 10^6$ s^{-1} and a diffusion coefficient of $D = 1.5 \times 10^{-9}$ cm^2/s. This relatively small barrier in the Z direction opens the possibility of V^0_{Li} diffusion under ambient conditions (For more details, see ref 36.)

We have conducted a similar analysis in Li_2CO_3, studying five different possible hops (see Figure 5). As it can be seen in Figure 5, the NEB calculations show low-energy barriers, that is, ~0.2 eV, for V^0_{Li} vacancy diffusion in all directions (X, Y, and Z). The most plausible diffusion channel follows the D → A hop in the Y direction, while the C → E hop is preferred in the Z direction and the A → B → C (D → A = B → C) hop

DOI: 10.1021/acs.jpcc.5b04432
J. Phys. Chem. C 2015, 119, 18066−18073

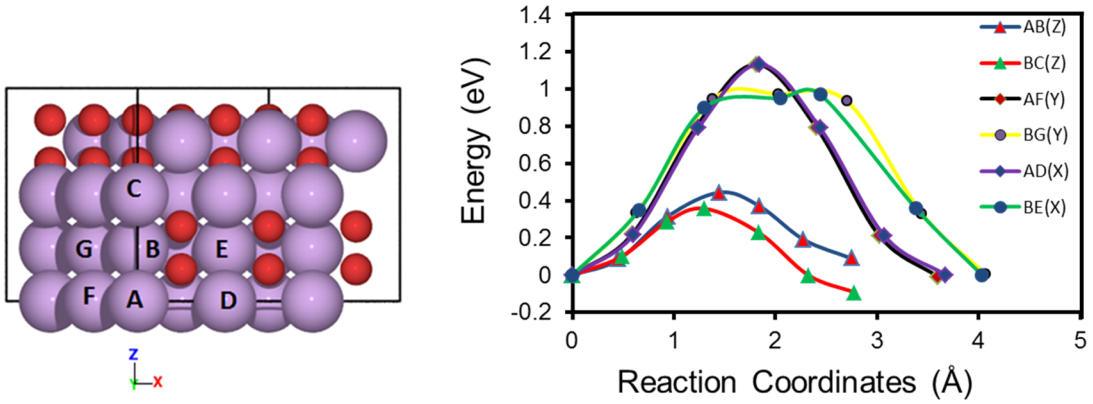

Figure 4. Calculated NEB paths for migration of neutral Li-vacancies, V^0_{Li}, following various diffusion paths in bulk Li_2O_2 using a 3 × 3 × 1 supercell. The minimum barrier is found to be 0.35 eV.

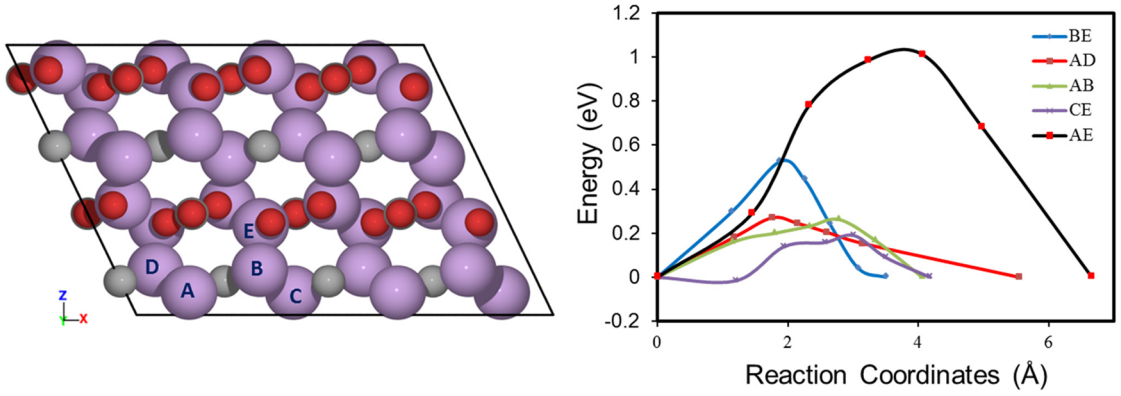

Figure 5. Calculated NEB paths for migration of neutral Li vacancies, V^0_{Li}, following various diffusion paths in bulk Li_2CO_3. The minimum barrier is found to be 0.20 eV.

sequence is favored in the X direction. The average rate (r) of Li vacancy diffusion in Li_2CO_3 yields $r = 9 \times 10^8$ s^{-1} with a corresponding diffusion coefficient of $D = 1.6 \times 10^{-6}$ cm^2/s.

The formation energies of V^0_{Li} vacancies relative to metallic lithium in Li_2O_2 bulk and Li_2CO_3 bulk are 3.00 and 4.20 eV, respectively, whereas the formation energies of V^0_{Li} vacancies at the Li_2O_2@Li_2CO_3 interface are 2.71 eV in the Li_2O_2 part of the interface and 3.24 eV in the Li_2CO_3 part. This means that in both materials vacancies will accumulate at the Li_2O_2@Li_2CO_3 interface rather than in their respective bulk. We have also calculated that there is no barrier to move V^0_{Li} vacancies from the Li_2CO_3 part of the interface to the Li_2O_2, suggesting that V^0_{Li} vacancies will tend to pile in the latter (see Figure 6). This also implies that the presence of the interface will not cause the ionic conductivity to become rate-limiting under practical operating conditions in Li−O_2 batteries.

The relatively large V^0_{Li} vacancy formation energy could lead us to think that the concentration of these vacancies should be negligible; however, it should be noted that the concentration of V^0_{Li} vacancies should be estimated using the formation energies at the working potentials of the battery. Varley et al.[35] and Radin et al.[36] have shown that at these potential V^0_{Li} vacancy formation energies are much lower, leading to a sufficient concentration to have significant ionic conduction.

3.2. Coherent Electron Transport in Li_2O_2 and Li_2O_2@Li_2CO_3 Interface. It is instructive to examine the density of states (DOS) of Li_2O_2 and Li_2CO_3 bulks and compare them with the one of the interface to have a comprehensive understanding of the coherent electron transport at the

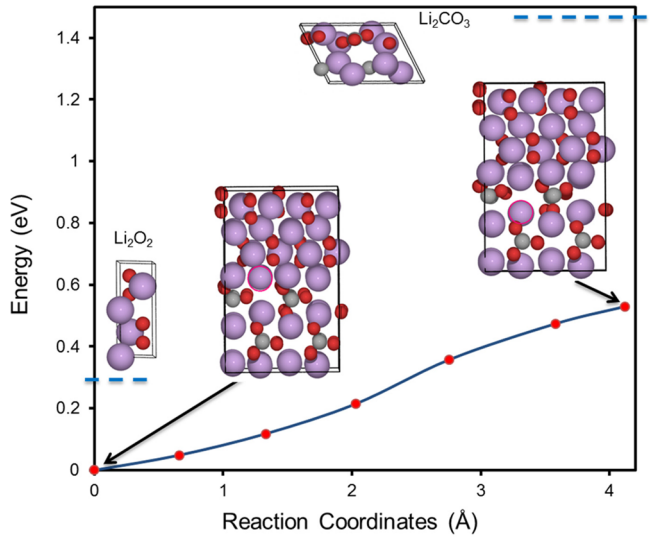

Figure 6. NEB calculations for the Li vacancy diffusion barrier at the $Li_2O_2(0001)$@$Li_2CO_3(011)$ interface. The thermodynamic barrier is found to be 0.53 eV going from the peroxide to the carbonate; the blue dashed lines represent the vacancy formation energies of bulk Li_2O_2 (+0.3 eV) and Li_2CO_3 (+∼1 eV) relative to the interface values.

Li_2O_2@Li_2CO_3 interface. In Figure 3 we can see that both Li_2O_2 and Li_2CO_3 are both wide bandgap insulators with calculated band gaps (using RPBE+U functional with U = 6 eV) of 5.03 eV for Li_2O_2 and 8.01 eV for Li_2CO_3. The Li_2O_2@

DOI: 10.1021/acs.jpcc.5b04432
J. Phys. Chem. C 2015, 119, 18066−18073

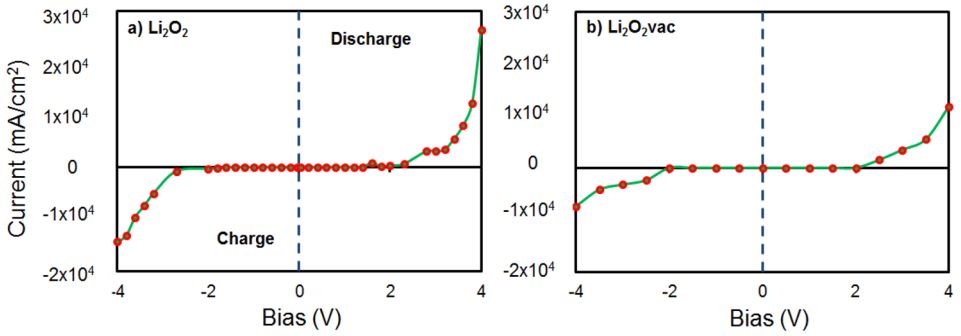

Figure 7. Calculated $I-V$ curves from ATK using the RPBE exchange correlation functional with k-point sampling $4 \times 6 \times 100$ using an electronic temperature of 300 K for (a) pristine Li_2O_2 and (b) in the presence of a neutral lithium vacancy.

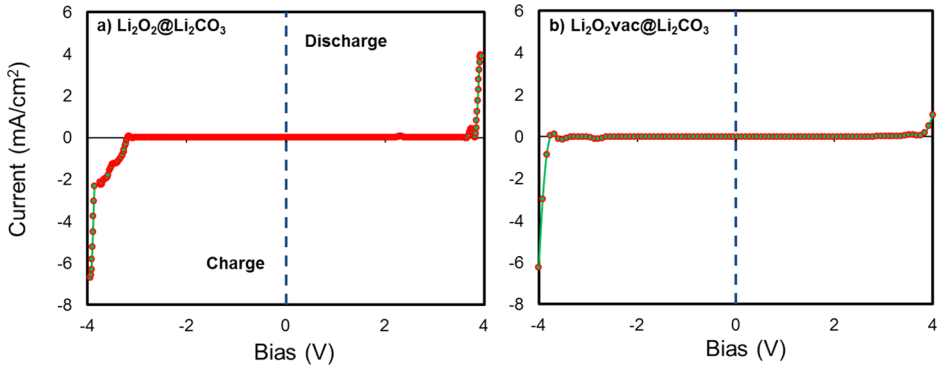

Figure 8. Calculated $I-V$ curves for (a) pristine $Li_2O_2(0001)@Li_2CO_3(011)$ and (b) with a neutral lithium vacancy at the $Li_2O_2(0001)$ vac@ $Li_2CO_3(011)$ interface.

Table 1. Energy Difference between the Localized (Polaron) and Delocalized States ($\Delta E_{loc\text{-}del}$) in Electronvolts for the Li_2O_2@ Li_2CO_3 Interface[a]

method	hole polaron in the Li_2O_2 part	hole polaron in the Li_2CO_3 part	electron polaron in the Li_2O_2 part	electron polaron in the Li_2CO_3 part
RPBE	delocalized	delocalized	delocalized	delocalized
RPBE+U (U = 6 eV)	−1.40	−0.57	−2.57	−2.67

[a]Hole and excess electron are localized at the Li_2O_2 and Li_2CO_3 parts of the interface using RPBE + U (U = 6 eV), as shown in Table 1.

Li_2CO_3 interface shows a 4.82 eV band gap (very close to the one of pristine Li_2O_2 bulk), and it can be viewed as the superposition of individual DOS of the Li_2O_2 and Li_2CO_3, with no presence of midgap interface states. In this situation it is expected that for bias voltages (negative or positive) around 2 to 2.5 eV (i.e., half of the bandgap of Li_2O_2) we will start to see a relative good conductance in the Li_2O_2 bulk; however, for the same bias we will expect a drastic drop in the conductance at the $Li_2O_2@Li_2CO_3$ interface because there are no Li_2CO_3 levels at these energies.

Regarding the presence of vacancies in Li_2O_2 bulk and at the $Li_2O_2@Li_2CO_3$ interface (vacancies are located at the Li_2O_2 part of the interface, following the results in Section 3), the DOS of both defect systems reveals that the vacancy levels pin the Fermi level of the pristine systems. This implies that V^0_{Li} vacancies are not going to open new electron tunneling channels in these systems, and they are going to have a detrimental effect in the conductivity due to their action as scattering centers.

To check the plausibility of these assumptions, we have performed DFT-NEGF calculations, as described in Section 2. We can see in Figure 7a that a significant current (~10 mA/cm^2) begins to show up just around ±2.0 V in pristine Li_2O_2 bulk; however, the current at the interface only starts rising at higher potentials (above ±3.80 V) due to the wider gap of Li_2CO_3 (see Figure 8). We also observe that the current at relevant voltages is reduced 3 orders of magnitude with respect to the one in Li_2O_2 bulk. Furthermore, V^0_{Li} vacancies reduce the currents at relevant voltages, of both Li_2O_2 bulk and $Li_2O_2@Li_2CO_3$ interface, by a factor of 2. In summary, we can conclude that the presence of $Li_2O_2@Li_2CO_3$ interfaces and V^0_{Li} vacancies in Li_2O_2 has a substantial negative effect on the coherent electronic transport at the oxygen electrode of Li−O_2 batteries.

3.3. Polaronic Transport in $Li_2O_2@Li_2CO_3$ Interface. We have already reported that both Li_2O_2 and Li_2CO_3 bulks can hold hole polarons with sufficiently low migration barriers (0.39 eV for the former and 0.55 eV for the latter) to become an alternative path for electronic transport.[37] We also found that both materials can hold excess electron polarons; however, the migration barriers for electron polarons are much higher than those of hole polarons (1.408 eV in Li_2O_2 and 1.05 in Li_2CO_3). Here we will focus on polaronic conduction (for both holes and excess electrons) at the $Li_2O_2@Li_2CO_3$ interface.

When we consider polaron localization at the Li_2O_2 part of the interface we observe that the hole (excess electron) polaron

DOI: 10.1021/acs.jpcc.5b04432
J. Phys. Chem. C 2015, 119, 18066−18073

is localized by shortening (stretching) the bond length of one of the O−O peroxide bond from 1.55 to 1.33 Å (2.45 Å). The localization can also take place at the Li_2CO_3 part of the interface. In this case the hole (excess electron) is localized in one of the carbonate ions that shortens (stretches) its C−O bond lengths from an average of 1.31 Å to an average of 1.23 Å (1.35 Å). Apart from the geometry distortions we observe in all of the cases the appearance of a magnetic moment in the oxyanions, which is another footprint of the hole (excess electron) localization. These localized states are more stable than the delocalized ones, and particularly the electron polaron is found to be strongly localized, that is, by >2 eV relative to the delocalized state (see Table 1). All of these features are very similar to the ones we found for Li_2O_2 and Li_2CO_3 bulks.[37]

It is interesting to notice that hole polarons are more stable in the Li_2O_2 part of the Li_2O_2@Li_2CO_3 interface by 0.83 eV, whereas the excess electron polarons are more stable in the Li_2CO_3 part by 0.10 eV (see Table 1 and Figure 9). This is due

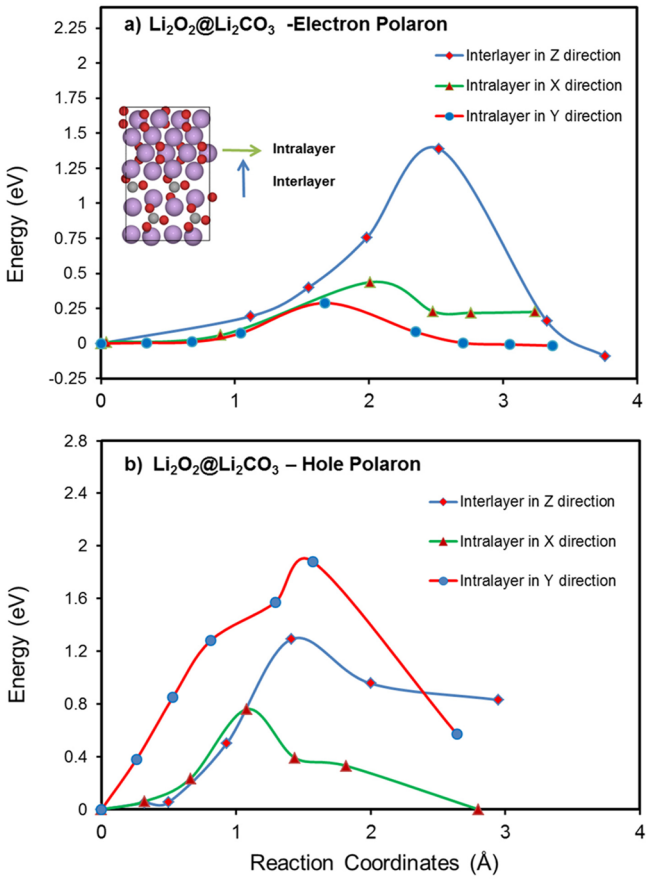

Figure 9. Calculated polaron hopping paths using the NEB method along the intralayer in X and Y directions and interlayer along Z direction in a 2 × 2 × 1 Li_2O_2@Li_2CO_3 interface supercell. Energies are obtained from RPBE + U (U = 6 eV) method for (a) excess electron and (b) hole.

to the different magnitude of the distortions in the peroxide ions of Li_2O_2; that is, a hole localized in a peroxide ion involves a change in the O−O bonding distance of 0.2 Å, while the localization of an excess electron requires stretching the bonding by 0.9 Å.

Accordingly to the NEB calculations, the energy barriers for the polaronic transport of excess electrons across the interface (see direction z in Figure 9) are very similar to the ones observed in Li_2O_2 and Li_2CO_3 bulks. The barrier for transporting excess electron polarons from Li_2O_2 to Li_2CO_3 is 1.39 eV (and 1.48 eV from Li_2CO_3 to Li_2O_2), very close to the 1.41 eV in Li_2O_2 bulk and 1.05 in Li_2CO_3 bulk. This implies that the excess electron polaronic transport across Li_2O_2@Li_2CO_3 interfaces is an inaccessible channel for electronic transport. The polaron hopping barrier for holes is much more asymmetric: the barrier for the hop from Li_2CO_3 to Li_2O_2 to is 0.4 eV (in Li_2O_2 bulk is 0.39 eV), while it is 1.3 eV in the opposite direction. In this scenario we can conclude that Li_2O_2@Li_2CO_3 interfaces act like a diode, which allows hole polaronic transport only from the Li_2CO_3 part of the interface to the Li_2O_2 one.

Regarding the polaronic transport parallel to the Li_2O_2@Li_2CO_3 interface we observe that an alternative channel for electron polaron hopping opens within the peroxide part of the interface (intralayer in the X and Y directions in Figure 9) with a low hopping barrier of <0.5 eV, providing an improved conduction channel compared with bulk Li_2O_2. The corresponding rates (r) in X and Y intralayer electron polaron hopping are found to be 5×10^5 and 9×10^7 s^{-1} with the diffusion coefficients of 5×10^{-10} and 1×10^{-7} cm^2/s, respectively. By contrast, the hole polaron hopping barriers parallel to the Li_2O_2@Li_2CO_3 interface are significantly larger compared with the low barriers reported for bulk Li_2O_2 by Garcia-Lastra et al.[37] (The barriers at the interface are at least two times larger than in bulk Li_2O_2.)

4. CONCLUSIONS

The detailed understanding of charge carrier transport across the Li_2O_2@Li_2CO_3 interfaces can shed new light on the limited performance of nonaqueous Li−O_2 batteries. DFT+U and NEGF's calculations have been applied to study the neutral lithium vacancy and electron/hole polaron migration barriers and I−V curves of the Li_2O_2 and Li_2O_2@Li_2CO_3 interface with and without defects. The role of Li vacancies in the cycling process is investigated and found to be prone to trapping at the peroxide part of the interface based on the relative vacancy formation energies, resulting in substantial reduction in the coherent transport. According to NEB calculations, the Li vacancy diffusion revealed low-energy barriers both across and parallel to the interface. The hole polaron conduction seems to be limited at the interface compared with values obtained for Li_2O_2.[37] The NEGF calculations also showed that the coherent transport is reduced due to the presence of interfaces and defects; however, low electron polaron hopping barriers are revealed in the plane parallel to the interface, opening an alternative conduction pathways, which may improve the electronic conduction under charge/discharge conditions, where the electron polaron formation energy is low and the concentration near the interface is consequently expected to be high.[35] Experimental realization of such well-defined interfaces may prove highly challenging, but this effect could possibly be investigated using nanostructured cathodes, (e.g., pillared graphene nanostructures as recently tested for Li-ion battery anodes[38]). In this case, alternating between electrochemical discharge (leading to Li_2O_2 formation) and short rest periods allowing some level of chemical degradation to form Li_2CO_3 inclusions should allow for a sufficient number of Li_2O_2@Li_2CO_3 interfaces capable of supplying the required electronic conduction to fill the space between the nanopillars.

DOI: 10.1021/acs.jpcc.5b04432
J. Phys. Chem. C 2015, 119, 18066−18073

AUTHOR INFORMATION

Corresponding Author

*E-mail: teve@dtu.dk.

Notes

The authors declare no competing financial interest.

ACKNOWLEDGMENTS

We acknowledge support of this work from the ReLiable project (project nr. 11-116792/0603-00462B) funded by the Danish Council for Strategic Research - Programme Commission on Sustainable Energy and Environment under the Danish Innovation Foundation, as well as the European Union's Seventh Framework Programme (FP7/2007-2013) under grant agreement no. 608575. J.M.G.-L. acknowledges support from the Spanish Ministry of Economy and Competitiveness under projects FIS2012-30996 and FIS2010-21282-C02-01 and from the Mat4Bat project founded by Villum Foundation Young Investigators Program (Project No. 10096). We also would like to thank Prof. Alan C. Luntz and Dr. Umberto M. Pozzoni for the constructive discussions we had.

REFERENCES

(1) Tarascon, J. M.; Armand, M. Issues and Challenges Facing Rechargeable Lithium Batteries. *Nature* **2001**, *414*, 359−367.

(2) Armand, M.; Tarascon, J. M. Building Better Batteries. *Nature* **2008**, *451*, 652−657.

(3) Balaish, M.; Kraytsberg, A.; Ein-Eli, Y. A Critical Review on Lithium-Air Battery Electrolytes. *Phys. Chem. Chem. Phys.* **2014**, *16*, 2801−2822.

(4) Mccloskey, B. D.; Speidel, A.; Scheffler, R.; Miller, D. C.; Viswanathan, V.; Hummelshøj, J. S.; Nørskov, J. K.; Luntz, A. C. Twin Problems of Interfacial Carbonate Formation in Nonaqueous Li−O_2 Batteries. *J. Phys. Chem. Lett.* **2012**, *3*, 997−1001.

(5) Younesi, R.; Hahlin, M.; Bjorefors, F.; Johansson, P.; Edstrom, K. Li−O_2 Battery Degradation by Lithium Peroxide (Li_2O_2): A Model Study. *Chem. Mater.* **2013**, *25*, 77.

(6) Xu, W.; Hu, J.; Engelhard, M. H.; Towne, S. A.; Hardy, J. S.; Xiao, J.; Feng, J.; Hu, M. Y.; Zhang, J.; Ding, F.; et al. The Stability of Organic Solvents and Carbon Electrode in Nonaqueous Li−O_2 Batteries. *J. Power Sources* **2012**, *215*, 240−247.

(7) Viswanathan, V.; Thygesen, K. S.; Hummelshøj, J. S.; Nørskov, J. K.; Girishkumar, G.; McCloskey, B. D.; Luntz, A. C. Electrical Conductivity in Li_2O_2 and Its Role in Determining Capacity Limitations in Non-Aqueous Li−O_2 Batteries. *J. Chem. Phys.* **2011**, *135*, 214704.

(8) Mekonnen, Y. S.; Knudsen, K. B.; Mýrdal, J. S. G.; Younesi, R.; Højberg, J.; Hjelm, J.; Norby, P.; Vegge, T. Communication: The Influence of CO_2 Poisoning on Overvoltages and Discharge Capacity in Non-Aqueous Li-Air Batteries. *J. Chem. Phys.* **2014**, *140*, 121101.

(9) Højberg, J.; McCloskey, B. D.; Hjelm, J.; Vegge, T.; Johansen, K.; Norby, P.; Luntz, A. C. An Electrochemical Impedance Spectroscopy Investigation of the Overpotentials in Li−O_2 Batteries. *ACS Appl. Mater. Interfaces* **2015**, *7*, 4039−4047.

(10) Albertus, P.; Girishkumar, G.; McCloskey, B.; Sánchez-Carrera, R. S.; Kozinsky, B.; Christensen, J.; Luntz, A. C. Identifying Capacity Limitations in the Li/Oxygen Battery Using Experiments and Modeling. *J. Electrochem. Soc.* **2011**, *158*, A343−A351.

(11) Shi, S.; Qi, Y.; Li, H.; Hector, L. G. Defect Thermodynamics and Diffusion Mechanisms in Li_2CO_3 and Implications for the Solid Electrolyte Interphase in Li-Ion Batteries. *J. Phys. Chem. C* **2013**, *117*, 8579−8593.

(12) Fracassi, P. F.; Klein, M. L.; Della Valle, R. G. Lattice Dynamics of Ionic Molecular Crystals in the Rigid Ion Approximation, Phases II and III of Sodium Superoxide. *Canada J. Phys.* **1984**, *62*, 54−64.

(13) Chen, J.; Hummelshøj, J. S.; Thygesen, K. S.; Myrdal, J. S. G.; Nørskov, J. K.; Vegge, T. The Role of Transition Metal Interfaces on the Electronic Transport in Lithium−air Batteries. *Catal. Today* **2011**, *165*, 2−9.

(14) Cota, L. G.; De La Mora, P. On the Structure of Lithium Peroxide, Li_2O_2. *Acta Crystallogr., Sect. B: Struct. Sci.* **2005**, *B61*, 133−136.

(15) Hummelshøj, J. S.; Blomqvist, J.; Datta, S.; Vegge, T.; Rossmeisl, J.; Thygesen, K.; Luntz, A. C.; Jacobsen, K. W.; Nørskov, J. K. Communication: Elementary Oxygen Electrode Reactions in the Aprotic Li-Air Battery. *J. Chem. Phys.* **2010**, *132*, 071101.

(16) Garcia-Lastra, J. M.; Bass, J. D.; Thygesen, K. S. Communication: Strong Excitonic and Vibronic Effects Determine the Optical Properties of Li_2O_2. *J. Chem. Phys.* **2011**, *135*, 121101.

(17) Radin, M. D.; Tian, F.; Siegel, D. J. Electronic Structure of Li_2O_2 {0001} Surfaces. *J. Mater. Sci.* **2012**, *47*, 7564−7570.

(18) Hummelshøj, J. S.; Luntz, a C.; Nørskov, J. K. Theoretical Evidence for Low Kinetic Overpotentials in Li−O_2 Electrochemistry. *J. Chem. Phys.* **2013**, *138*, 034703.

(19) Effenberger, H.; Zemann, J. Refining the Crystal-Structure of Lithium-Carbonate, Li_2CO_3. *Z. Kristallogr.* **1979**, *150*, 133−138.

(20) Mo, Y.; Ong, S. P.; Ceder, G. First-Principles Study of the Oxygen Evolution Reaction of Lithium Peroxide in the Lithium-Air Battery. *Phys. Rev. B: Condens. Matter Mater. Phys.* **2011**, *84*, 205446.

(21) Bruno, M.; Prencipe, M. Ab Initio Quantum-Mechanical Modeling of the (001), and (110) Surfaces of Zabuyelite (Li_2CO_3). *Surf. Sci.* **2007**, *601*, 3012−3019.

(22) Ernzerhof, M.; Scuseria, G. E. Perspective on "Inhomogeneous Electron Gas". *Theor. Chem. Acc.* **2000**, *103*, 259−262.

(23) Kohn, W.; Sham, L. J. Self-Consistent Equation Including Exchange and Correlation Effects. *Phys. Rev.* **1965**, *140*, A1133−A1138.

(24) Mortensen, J. J.; Hansen, L. B.; Jacobsen, K. W. A Real-Space Grid Implementation of the Projector Augmented Wave Method. *Phys. Rev. B: Condens. Matter Mater. Phys.* **2005**, *71*, 035109.

(25) Enkovaara, J.; Rostgaard, C.; Mortensen, J. J.; Chen, J.; Dułak, M.; Ferrighi, L.; Gavnholt, J.; Glinsvad, C.; Haikola, V.; Hansen, H. a; et al. Electronic Structure Calculations with GPAW: A Real-Space Implementation of the Projector Augmented-Wave Method. *J. Phys.: Condens. Matter* **2010**, *22*, 253202.

(26) Bahn, S. R.; Jacobsen, K. W. An Object-Oriented Scripting Interface to a Legacy Electronic Strcture Code. *Comput. Sci. Eng.* **2002**, *4*, 56−66.

(27) Blochl, P. E. Projected Augmented-Wave Method. *Phys. Rev. B: Condens. Matter Mater. Phys.* **1994**, *50*, 17953−17979.

(28) Hammer, B.; Hansen, L.; Nørskov, J. Improved Adsorption Energetics within Density-Functional Theory Using Revised Perdew-Burke-Ernzerhof Functionals. *Phys. Rev. B: Condens. Matter Mater. Phys.* **1999**, *59*, 7413−7421.

(29) Henkelman, G.; Jonsson, H. Improved Tangent Estimate in the Nudged Elastic Band Method for Finding Minimum Energy Paths and Saddle Points. *J. Chem. Phys.* **2000**, *113*, 9978−9985.

(30) Hanggi, P.; Talkner, P.; Borkovec, M. Reaction-Rate Theory: Fifty Years after Kramers. *Rev. Mod. Phys.* **1990**, *62*, 251−342.

(31) Vegge, T.; Rasmussen, T.; Leffers, T.; Pedersen, O.; Jacobsen, K. Determination of the of Rate Cross Slip of Screw Dislocations. *Phys. Rev. Lett.* **2000**, *85*, 3866−3869.

(32) Atomistix ToolKit version 2014.1, QuantumWise A/S (www.quantumwise.com).

(33) Brandbyge, M.; Mozos, J.-L.; Ordejón, P.; Taylor, J.; Stokbro, K. Density-Functional Method for Nonequilibrium Electron Transport. *Phys. Rev. B: Condens. Matter Mater. Phys.* **2002**, *65*, 165401.

(34) Soler, J. M.; Artacho, E.; Gale, J. D.; Garcia, A.; Junquera, J.; Ordejon, P.; Sanchez-Portal, D. The SIESTA Method for Ab Initio Order-N Materials Simulation. *J. Phys.: Condens. Matter* **2002**, *14*, 2745−2779.

(35) Varley, J. B.; Viswanathan, V.; Nørskov, J. K.; Luntz, a. C. Lithium and Oxygen Vacancies and Their Role in Li_2O_2 Charge Transport in Li−O_2 Batteries. *Energy Environ. Sci.* **2014**, *7*, 720−727.

DOI: 10.1021/acs.jpcc.5b04432
J. Phys. Chem. C 2015, 119, 18066−18073

(36) Radin, M. D.; Siegel, D. J. Charge Transport in Lithium Peroxide: Relevance for Rechargeable Metal−air Batteries. *Energy Environ. Sci.* **2013**, *6*, 2370−2379.
(37) Garcia-Lastra, J. M.; Myrdal, J. S. G.; Christensen, R.; Thygesen, K. S.; Vegge, T. DFT+U Study of Polaronic Conduction in Li_2O_2 and Li_2CO_3: Implications for Li-Air Batteries. *J. Phys. Chem. C* **2013**, *117*, 5568−5577.
(38) Wang, W.; Ruiz, I.; Guo, S.; Favors, Z.; Bay, H. H.; Ozkan, M.; Ozkan, C. S. Hybrid Carbon Nanotube and Graphene Nanostructures for Lithium Ion Battery Anodes. *Nano Energy* **2014**, *3*, 113−118.

DOI: 10.1021/acs.jpcc.5b04432
J. Phys. Chem. C 2015, 119, 18066−18073